Journal of Power Sources 268 (2014) 584–590

Contents lists available at ScienceDirect

Journal of Power Sources

journal homepage: www.elsevier.com/locate/jpowsour

Micro-mesoporous carbon spheres derived from carrageenan as electrode material for supercapacitors

Yang Fan*, Xin Yang, Bing Zhu, Pei-Fang Liu, Hai-Ting Lu

College of Chemistry and Chemical Engineering, Xinyang Normal University, Xinyang 464000, China

HIGHLIGHTS

- Carrageenan was used as a natural precursor to prepare porous carbon spheres.
- The carbon spheres have high surface area of 2502 $m^2\ g^{-1}$.
- The carbon spheres possess well-controlled micro- and mesoporosity.
- The micro-mesoporous carbon spheres exhibited superior capacitive performance.

ARTICLE INFO

Article history:
Received 9 February 2014
Received in revised form
18 June 2014
Accepted 18 June 2014
Available online 25 June 2014

Keywords:
Carrageenan
Micro-mesoporous
Carbon spheres
Supercapacitors
Biomass

ABSTRACT

The polysaccharide carrageenan is used as a natural precursor to prepare micro-mesoporous carbon spheres. The carbon spheres were synthesized by hydrothermal carbonization of carrageenan, and subsequent chemical activation by KOH at different temperatures. The obtained micro-mesoporous carbon spheres have high surface area (up to 2502 $m^2\ g^{-1}$) and large pore volume (up to 1.43 $cm^3\ g^{-1}$). Moreover, the micro- and mesoporosity can be finely tuned be modifying the activation temperatures in the range of 700–900 °C. The carbon spheres activated at 900 °C present high specific capacitance of 230 F g^{-1} at a current density of 1 A g^{-1} and good ion transport kinetics. The good capacitive performance can be ascribed to the high specific surface area, well-controlled micro- and mesoporosity and narrow pore size distribution.

1. Introduction

Biomass-derived porous carbons have recently shown promising application as electrode material for supercapacitors [1–13]. Various kinds of biomass, such as seaweeds, coconut shell, leaves, rice husk, fugi and so forth, have been investigated as the carbon source to develop advanced carbon materials. These carbon materials exhibited favorable electrochemical capacitance performances which are comparable or superior to that of state-of-the art activated carbons, carbon nanotubes and graphene. More importantly, the development of carbon-based energy materials using the renewable biomass is an environmentally sustainable way as compared to that using the diminishing fossil resource [14,15].

Carrageenan is a family of high molecular weight sulfated polysaccharides obtained by extraction of certain species of red seaweeds [16]. It is composed of galactose and anhydrogalactose units linked by glycosidic unions. Due to its special characteristics such as gelling, emulsifying and stabilizing abilities, carrageenan has been extensively used as stabilizer and excipient in food and pharmaceutical industry [16]. However, to the best of our knowledge, this natural polysaccharide has not been used as the carbon source to prepare carbon material for energy-related applications. Recently, Encarnación and co-workers used the Lessonia Nigrescens brown seaweed as the natural precursor to prepare porous carbons [17]. Direct pyrolysis of the brown seaweeds produced porous carbons with moderate specific surface area and tuned porosity which exhibited good capacitance performance. As well-known, seaweeds are the most abundant resource of multiple polysaccharides such as carrageenan, alginate and agar. Owing to their abundance (7.5–8 million tons per year) and renewability, seaweeds and its derivatives are promising and sustainable carbon sources for carbon materials towards energy and environmental applications.

* Corresponding author. Tel./fax: +86 376 6391825.
E-mail address: yfanchem@163.com (Y. Fan).

http://dx.doi.org/10.1016/j.jpowsour.2014.06.100
0378-7753/

Porous carbons with well-controlled micro- and mesoporosity have attracted growing interests due to their superior capacitive properties [18–23]. It is known that both efficient electrosorption of electrolyte ion for the electric double-layer formation and the fast ion transport within porous textures are critically important to achieve higher capacitive performance [24–27]. As for the micro-mesoporous carbon materials, it revealed that the incorporating of abundant micropores with interconnected mesopores is favorable to achieve both large charge storage density and short ion transport distance [18,23]. However, hard templates (*e.g.* SAB-15, CMK-3, MCM-48, *etc.*) are generally used to introduce mesoporous structure into the carbon framework. This template technique usually involves tedious and multistep procedures, and even non-environmentally friendly conditions. In this study, carrageenan was used as the natural precursor to synthesize porous carbon spheres with well-controlled micro- and mesoporosity. The micro-mesoporous carbon spheres were synthesized by hydrothermal carbonization of carrageenan, and the subsequent chemical activation by KOH [28,29]. The carrageenan-derived carbon spheres possess high surface area, well-balanced micro- and mesoporosity, and controlled pore size distribution. Owing to the unique structure and porosity, the carrageenan-derived carbon spheres exhibit high specific capacitance, with good rate capabilities and cycling stability.

2. Experimental

2.1. Reagents

Carrageenan (reagent grade), KOH (analytical grade) and polytetrafluoroethylene (PTFE, 60 wt % dispersion in water) were purchased from Aladdin Reagent Inc. All the chemicals were used as received without further purification.

2.2. Synthesis

In a typical procedure, carrageenan (3 g) was dissolved in water (50 mL) under stirring. The resulting solution was sealed into a Teflon-lined autoclave of 100 mL capacity and maintained at 200 °C for 12 h. After the autoclave was cooled to room temperature, the obtained hydrothermal carbon (denoted as HC-200) as dark precipitate were collected by centrifugation, washed with water and ethanol for several times, and dried in vacuum at 70 °C for 8 h. The obtained hydrothermal carbon was then chemically activated by KOH at temperatures in the range of 700–900 °C with the HC-200/KOH weight ratio of 1:3. The mixture was heated in tube furnace under N_2 atmosphere for 2 h, with a temperature ramp of 5 °C min^{-1}. The obtained activated carbon was washed with 2 M hydrochloric acid and water to remove potassium species thoroughly, and finally dried at 110 °C in an electric oven overnight. The as-synthesized carbon spheres with activation temperature of 700, 800 and 900 °C were denoted as AC-700, AC-800 and AC-900, respectively.

2.3. Characterizations

Scanning electron microscopy (SEM) images were recorded on a Hitachi S-4800 field-emission scanning electron microscope. Transmission electron microscopy (TEM) images and high-resolution TEM (HR-TEM) images were obtained on a FEI Tecnai G2 microscope operated at 200 kV; the samples were dispersed in ethanol and dropped on a lacey carbon coated copper grid. X-ray diffraction (XRD) patterns were recorded on a Rigaku MiniFlex600 X-ray diffractometer with Cu Kα radiation ($\lambda = 1.5418$ Å) operating at 40 kV, 15 mA. The data were collected from 5 to 90° with the scan rate of 2° min^{-1} and steps of 0.02°. Raman spectra were recorded by a LabRAM HR Raman spectrometer with a 514.5 nm laser excitation. N_2 adsorption–desorption isotherms at 77 K were measured using

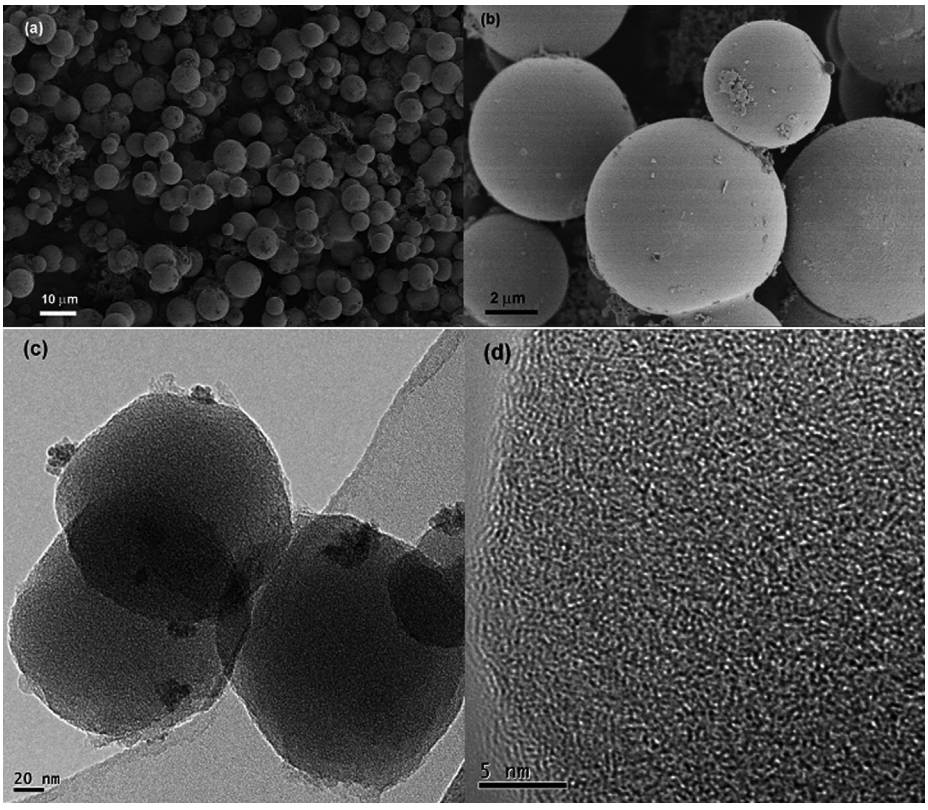

Fig. 1. SEM images of (a) HC-200 and (b) AC-900; (c) TEM and (d) HR-TEM images of AC-900.

an Autosorb-iQ automated gas sorption analyzer (Quantachrome Instrument). The specific surface area was calculated by the Brunauer–Emmett–Teller (BET) method. The total pore volume was calculated from the amount of nitrogen adsorbed at a relative pressure (P/P_0) of 0.99. The pore size distribution (PSD) curve of the hydrothermal carbon sample HC-200 was retrieved with the Barrett–Joyner–Halenda (BJH) model by using the adsorption branch. The PSD of activated carbon spheres is calculated from the adsorption branch of the isotherm by the Quenched Solid Density Functional Theory (QSDFT) method.

2.4. Electrochemical tests

The electrochemical experiments were performed with a CHI 660E electrochemical analyzer (CH Instruments). A three-electrode system was used, which consisted of a platinum wire as counter electrode, a saturated calomel electrode (SCE) as reference electrode, and a working electrode. The working electrode was prepared by mixing the carbon samples, acetylene black and polytetrafluoroethylene (PTEF) in the ratio of 75:15:10, and pressing (20 MPa) the mixture onto nickel foam (1×1 cm^2) with mass loading of 3 mg. The electrolyte was a 6 M KOH aqueous solution. Cyclic voltammetry (CV) curves were obtained in the potential range of −1.1 to −0.1 V vs. SCE by varying the scan rate from 5 to 100 mV s^{-1}. Charge–discharge measurements were done galvanostatically at 0.5–10 A g^{-1} over a voltage range of −1.1 to −0.1 V vs. SCE. Electrochemical impedance spectroscopy (EIS) was measured in a frequency range of 10^{-3} to 10^6 Hz at open circuit voltage with amplitude of 5 mV.

Table 1
Textural properties of the carrageenan derived carbon spheres.

Sample	S_{BET}[a] ($m^2\ g^{-1}$)	S_{micro}[b] ($m^2\ g^{-1}$)	V_{total}[c] ($cm^3\ g^{-1}$)	V_{micro}[b] ($cm^3\ g^{-1}$)	V_{meso}[d] ($cm^3\ g^{-1}$)
HC-200	14	0	0.036	0	0.036
AC-700	1865	1562	1.10	0.80	0.12
AC-800	2236	1759	1.39	0.90	0.28
AC-900	2502	1836	1.43	0.90	0.43

[a] Total surface area calculated using the BET method.
[b] Micropore surface area and volume calculated from *t*-plot method.
[c] Total pore volume calculated at $P/P_0 = 0.99$.
[d] Mesopore volume was calculated as the difference between the pore volume at $P/P_0 = 0.95$ and $P/P_0 = 0.10$.

3. Results and discussion

As shown in Fig. 1a, the hydrothermal carbonization of carrageenan produced carbon spheres with diameter of 3–6 μm. This kind of spherical micro-sized particles was commonly observed for the hydrothermal carbons derived from mono- and polysaccharides (*e.g.* glucose, sucrose, starch and cellulose) [14]. Upon KOH activation, the spherical morphology of the hydrothermal

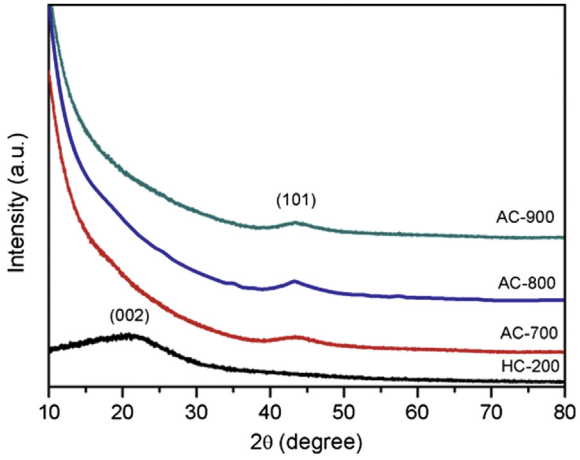

Fig. 2. XRD patterns of HC-200 and the activated carbon spheres.

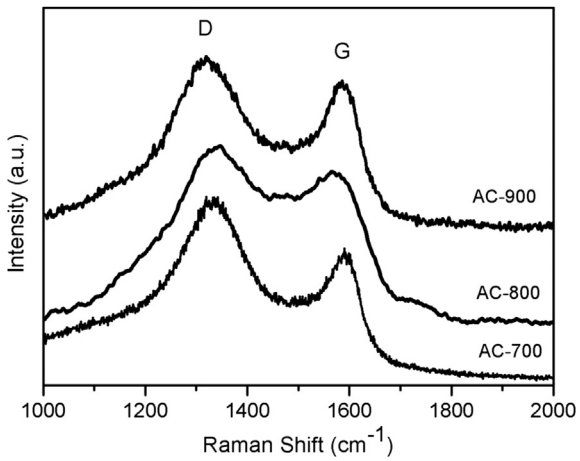

Fig. 3. Raman spectra of the activated carbon spheres.

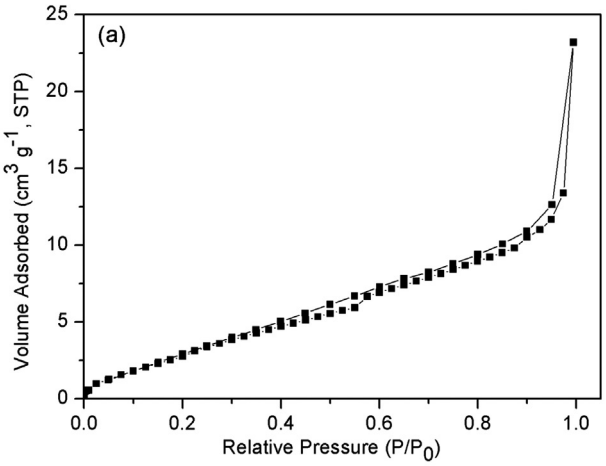

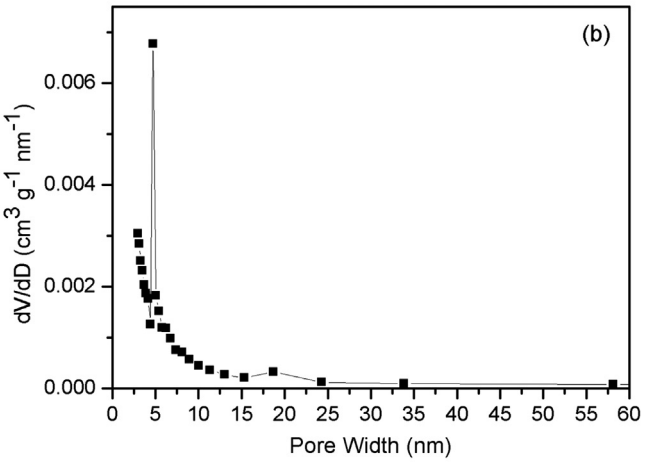

Fig. 4. (a) N_2 adsorption–desorption isotherms and (b) pore size distribution of HC-200.

carbon was still maintained in obtained activated carbon, as evidenced by the SEM and the TEM images (Fig. 1a–c). This behavior is similar with that of the glucose and cellulose derived hydrothermal carbons which could maintain their spherical morphology when the KOH/hydrothermal carbon ratio is lower than 4/1 [30]. The HR-TEM image (Fig. 1d) corresponding to the surface of carbon sphere indicates the amorphous nature of the activated carbon [31,32].

XRD patterns (Fig. 2) of the hydrothermal carbon (HC-200) shows single broad peak around 21.5° corresponding to the (002) interlayer reflection, indicating the presence of amorphous nature and low graphitization. The activated carbon spheres prepared at different temperatures exhibit similar XRD patterns with a weak reflection centered at 43.5°, corresponding to (101) in-plane scattering. This demonstrates that the level of structure order for the hydrothermal carbon improves towards a turbostatic structure after high temperature carbonization, as reported by Titirici et al. for the chitosan derived hydrothermal carbon [33]. Fig. 3 depicts the typical Raman spectra of the activated carbon spheres. The peaks located at around 1320 and 1585 cm^{-1} are assigned to the characteristic D (defects and disorder) and G (graphitic) bands of carbon materials, respectively [34,35]. The G/D ratio of band intensities indicates the graphitic structure with respect to the degree of structural disorder and defects [35]. The G/D intensity ratio of AC-700, AC-800 and AC-900 were determined to be about 0.7, 0.9 and 0.9, respectively. This result indicates that the high temperature carbonization increases the degree of the graphitization [11]. Based on the XRD and Raman spectra analysis, it can be seen that the microstructure of carbon samples with spherical morphology was modulated by the carbonization and activation treatments.

The porosity of the as-prepared hydrothermal carbon and the activated carbon spheres were analyzed by N_2 sorption technique (Table 1). The N_2 adsorption–desorption isotherm curve of the hydrothermal carbon HC-200 displays type-IV isotherm with H3 type hysteresis loop, showing the characteristics of a mesoporous material with the presence of slit-shaped pores (Fig. 4a). Moreover, the isotherm presents a sharp increase in the N_2 uptake at high relative pressures ($p/p_0 > 0.9$), indicating the existence of macropores in the sample [36]. The PSD plot calculated by the Barrett–Joyner–Halenda (BJH) method is shown in Fig. 4b. It can be seen that the HC-200 sample has a PSD centered at about 5 nm. The Brunauer–Emmett–Teller (BET) specific surface area of the HC-200 sample is calculated to be 14 $m^2 g^{-1}$. The low surface area of HC-200 is comparable to that of previously reported hydrothermal carbons derived from natural polysaccharides, which is not suitable for supercapacitor application [14,15].

Fig. 5a shows the N_2 adsorption–desorption isotherms of the activated carbon spheres prepared by KOH activation of the hydrothermal carbon HC-200 at various temperatures in the range of

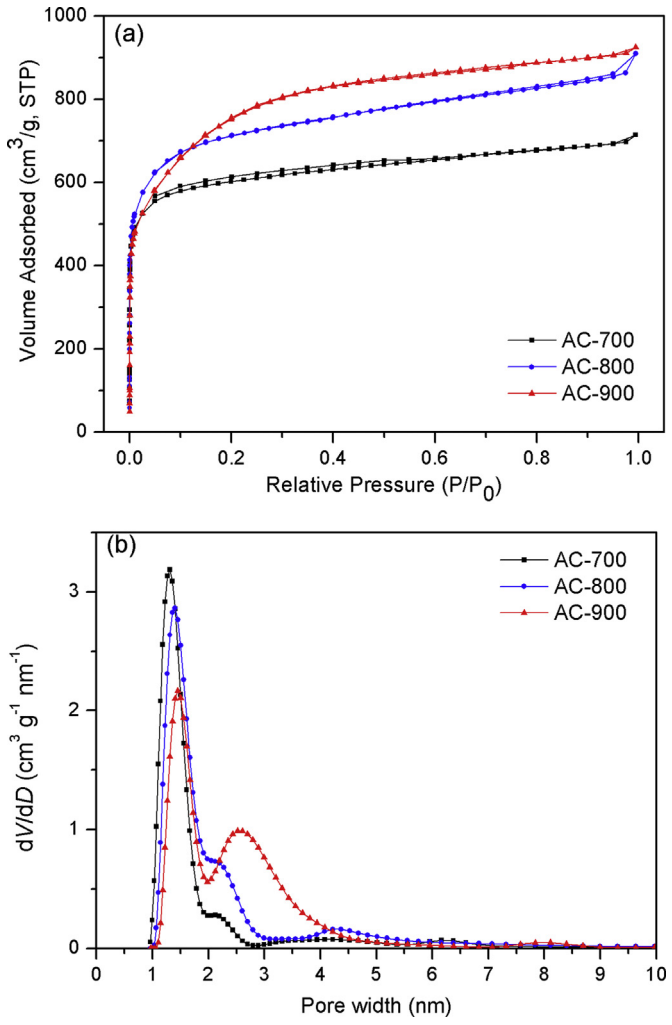

Fig. 5. (a) N_2 adsorption–desorption isotherms and (b) pore size distribution of the activated carbon spheres.

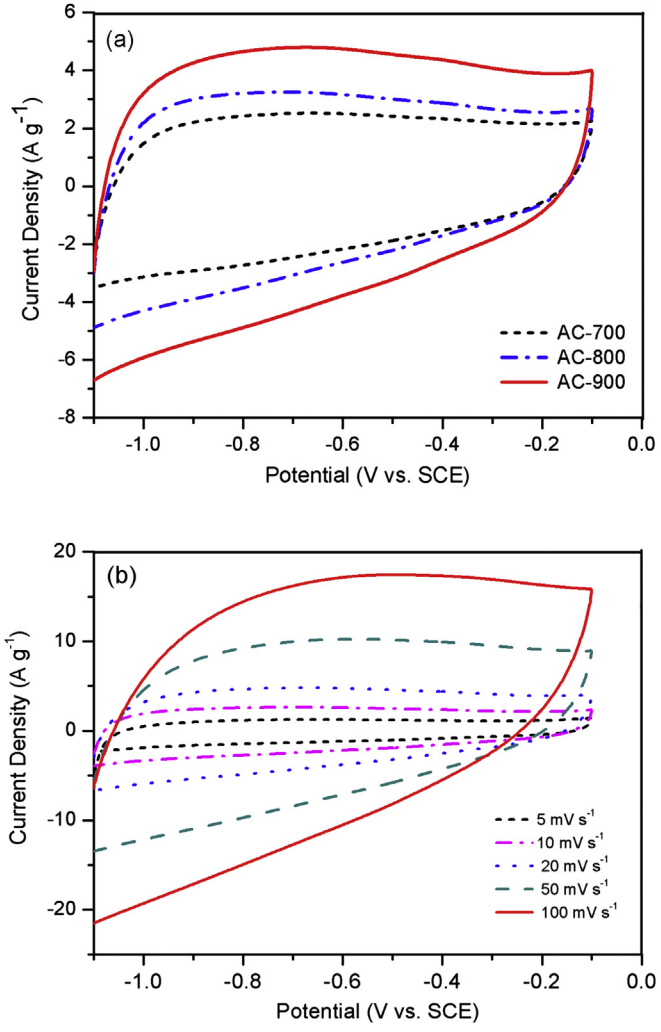

Fig. 6. CV curves of (a) the activated carbon spheres at 20 mV s^{-1} and (b) AC-900 at various scan rates ranging from 5 to 100 mV s^{-1}.

700–900 °C. The steep increase in volume adsorbed at low relative pressure reflects the high micropore content of these activated carbons. As for AC-900, besides the high N_2 uptake at low relative pressure, the additional N_2 uptake at $P/P_0 = 0.2–0.5$ indicates the presence of mesopores. Compared to the hydrothermal carbon HC-200, the surface area and pore volume were remarkably increased through KOH activation. Apparently, the porosity was effectively developed by KOH activation [15,28,29]. The influence of activation temperature on the porosity of activated carbon spheres was investigated. The surface area and the total pore volume increase from 1865 $m^2\ g^{-1}$ and 1.1 $cm^3\ g^{-1}$ at 700 °C to 2502 $m^2\ g^{-1}$ and 1.43 $cm^3\ g^{-1}$ at 900 °C. The specific surface area of AC-900 carbon spheres is close to the theoretical surface area of graphene (2630 $m^2\ g^{-1}$) [37], and about 2 times higher than that of the porous carbon synthesized using row biomass brown seaweeds as precursor [17]. The PSD is calculated from the adsorption branch of the isotherm by the Quenched Solid Density Functional Theory (QSDFT) method [38]. The QSDFT method offers a major improvement of the accuracy of DFT pore size distribution analyses of geometrically and chemically disordered micro-mesoporous carbons. As shown in Fig. 5b, the AC-700 and AC-800 carbon spheres present high ratio of micropores and nearly mono-modal PSD with peak at 1.3 and 1.4 nm, respectively. In contrast, the AC-900 carbon spheres exhibits a typical bimodal PSD curve which contains a sharp peak at 1.5 nm and a broad peak around 2.6 nm. It can be seen that higher activation temperature trends to enlarge the pore size and increase the volume of mesopores. This can be ascribed to the gasification of the hydrothermal carbon by CO_2 which was generated form the decomposition of K_2CO_3 in the activation process [28,29].

The electrochemical capacitive properties of the carrageenan-derived carbon materials were measured in 6 M KOH using three-electrode system. Fig. 6a depicts the CV curves for the carbon spheres at a scan rate of 20 mV s^{-1}. The CV curves of activated carbon spheres display a quasi-rectangular shape, showing a typical characteristic of double-layer capacitance. Among the carbon spheres, AC-900 exhibit CV curve with the largest area of loop, suggesting the highest capacitance. Moreover, as can be seen from Fig. 6b, AC-900 still presents a relatively rectangular CV shape at a high scan rate of 100 mV s^{-1}, implying efficient charge transfer and electrolyte diffusion within the porous carbon spheres [1].

The galvanostatic charge–discharge curves of the carbon spheres at current density of 1 A g^{-1} are shown in Fig. 7a. The triangular shape curves indicate excellent electrochemical reversibility of the carbon spheres. The specific capacitance was calculated according to the following equation: $C = i\Delta t/m\Delta V$, where i is the discharge current (A), Δt is the discharge time (s), and ΔV is the potential window (V) [6]. The obtained specific capacitance values are 160, 192 and 230 F g^{-1} at current density of 1 A g^{-1} for AC-700, AC-800 and AC-900, respectively. Fig. 7b shows the galvanostatic charge–discharge curves of AC-900 carbon spheres at different current densities. At a high current density of 10 A g^{-1}, AC-900 shows a capacitance of 152 F g^{-1} which preserves 67% of its capacitance delivered at 1 A g^{-1}, indicating favorable capacitance retention (Fig. 7c). Among the carbon spheres, the highest specific capacitance of AC-900 can be ascribed to the highest specific surface area resulting from the abundant micropores (S_{micro} = 1837 $m^2\ g^{-1}$ and V_{micro} = 0.9 $cm^3\ g^{-1}$), which was critical to the charge storage. To evaluate the cycle stability of the AC-900 electrode, the continuous charge–discharge process was conducted at a current density of 1 A g^{-1} for 1000 cycles (Fig. 7d). About 95% of specific capacitance was retained after 1000 galvanostatic charge–discharge cycles, demonstrating good cycling stability. In comparison with the recently reported carbon sphere electrode materials which were commonly synthesized by template methods (Table 2) [39–45], the carrageenan-derived carbon spheres show the highest surface area and very competitive capacitance of

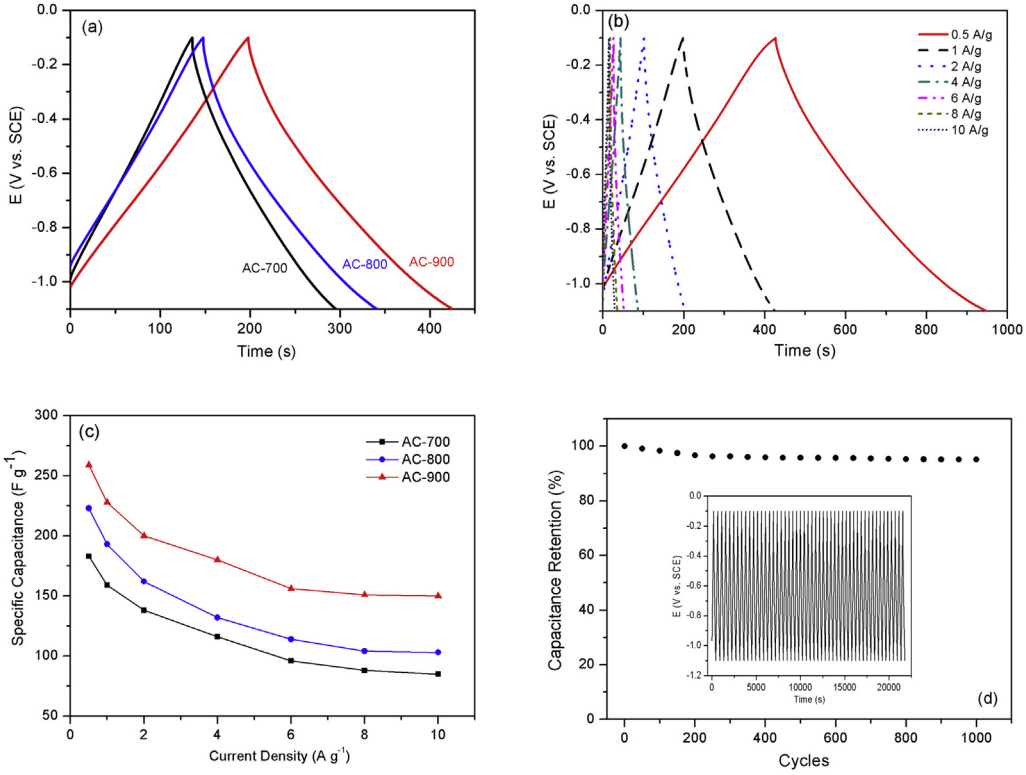

Fig. 7. Galvanostatic charge–discharge curves of (a) the activated carbon spheres at current density of 1 A g^{-1} and (b) AC-900 at different current densities (0.5–10 A g^{-1}); (c) specific capacitance of the activated carbon spheres at different current densities (0.5–10 A g^{-1}), (d) cycle stability of AC-900 at current density of 1 A g^{-1}.

Table 2
Carbon spheres for supercapacitor electrodes.

Material	Carbon source	S_{BET} ($m^2\ g^{-1}$)	Specific capacitance ($F\ g^{-1}$)[a]	Electrolyte	Ref.
HMCNs[b]	Dopamine	568	253 (1 A g^{-1})	1 M H_2SO_4	[39]
HCMSs[c]	Phenol-formaldehyde	1704	251 (50 mV s^{-1})	2 M H_2SO_4	[40]
MCS[d]	Ferrocene	2396	225 (0.25 A g^{-1})	6 M KOH	[41]
GR hollow spheres	Graphene oxide	440	273 (0.5 A g^{-1})	5 M KOH	[42]
Porous carbon spheres	Glucose	757.3	260 (0.5 A g^{-1})	6 M KOH	[43]
Hollow carbon spheres	Resorcinol-formaldehyde	1286	210 (1 A g^{-1})	1 M KOH	[44]
PNHS[e]	Polyaniline	213	213 (0.5 A g^{-1})	6 M KOH	[45]
Carbon spheres	Carrageenan	2502	261 (0.5 A g^{-1})	6 M KOH	This work

[a] Three-electrode cell.
[b] Hollow mesoporous carbon nanospheres.
[c] Hollow core, mesoporous shell carbon nanospheres.
[d] Mesoporous carbon nanospheres.
[e] Porous nitrogen-doped hollow carbon spheres.

261 F g^{-1} at 0.5 A g^{-1}. This demonstrates that carbon sphere material with high surface area, tunable porosity and superior capacitive performance can be obtained from carrageenan using the simple and template-free synthetic method.

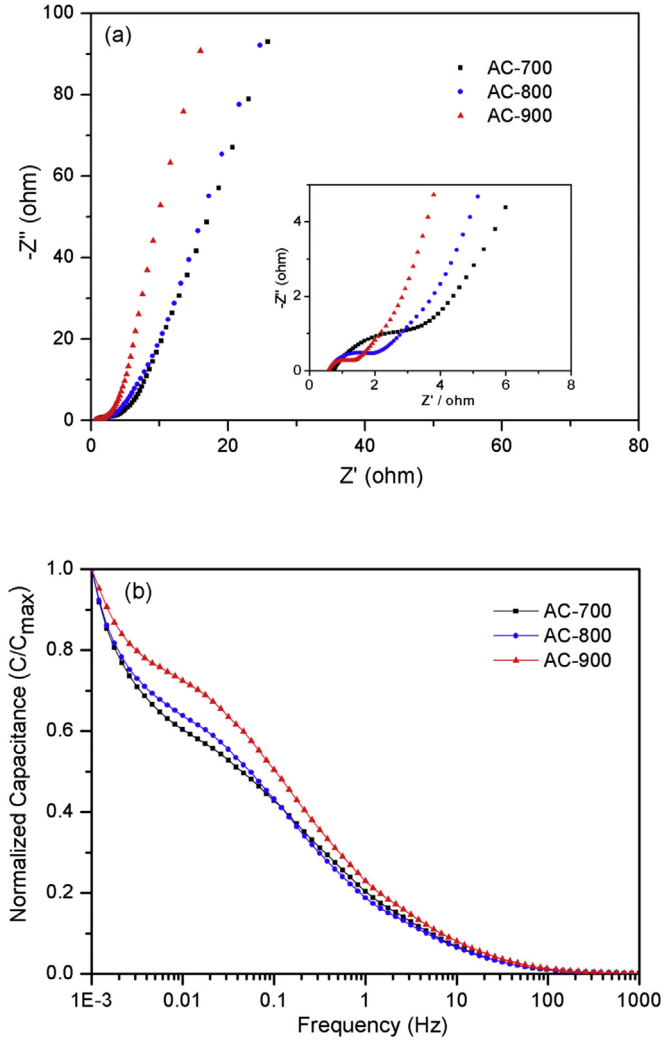

Fig. 8. (a) Nyquist plots of the activated carbon spheres. The inset shows the magnified view of the high-frequency region; (b) Frequency responses of the activated carbon spheres.

Fig. 8a shows the Nyquist plots obtained for the carbon spheres in the frequency range of 10^{-3}–10^{6} Hz under open circuit potential. The carbon spheres display good capacitive behavior with vertical slope at the low-frequency region. At high frequency, the intercept of plot with real axis represents the equivalent series resistance (ESR) R_s which is a combination of the ionic resistance of the electrolyte, intrinsic resistance of the active materials, and contact resistance with the current collector [1]. AC-900 exhibits R_s value of 0.58 Ω, which is lower than that of 0.61 and 0.73 Ω for AC-800 and AC-700, respectively. At medium frequencies, Nyquist plots exhibit Warburg-type line with a slope of about 45°. The diffusion of ions at the electrode–electrolyte interface could be evaluated by the projected length of the Warburg line on the real axis [7]. As shown in the insert of Fig. 8a, the AC-900 demonstrates the shortest Warburg-type line, indicating superior ion diffusion in the micro-mesoporous structure of AC-900. Bode plots of the frequency response of capacitance are presented in Fig. 8b. The operating frequency at half maximum capacitance (f_{max}) of AC-900 is 0.12 Hz, which is higher than those of AC-700 (0.04) and AC-800 (0.05). The faster frequency response AC-900 can be ascribed to its higher mesoporosity which favors the electrolyte ions transportation [12]. Moreover, the AC-900 possesses a much narrow mesopore distribution in the range of 2–5 nm which is primarily responsible for facilitating the access of electrolyte ion into the micropores of electrode material [18,23].

4. Conclusions

In summary, micro-mesoporous carbon spheres were synthesized by using carrageenan as natural precursor. KOH activation of the carrageenan-derived hydrothermal carbon produced carbon spheres with high specific surface area (up to 2502 $m^2\ g^{-1}$), large pore volumes (up to 1.43 $cm^3\ g^{-1}$). Moreover, it shows that the micro- and mesoporosity can be easily modulated by the activation temperatures. Among the as-synthesized carbon spheres, the AC-900 presented the best capacitive performance with specific capacitance of 230 F g^{-1} at a current density of 1 A g^{-1}, as well as good ion transport kinetics with operating frequency of 0.12 Hz. The superior capacitive properties of AC-900 carbon spheres are closely related to its high surface area, optimized micro- and mesoporous structure and narrow PSD. This work demonstrates that the textural properties of carbon materials derived from biomass can be finely modulated by KOH activation. The carrageenan-derived carbon sphere materials have promising potential in application of energy storage devices.

Acknowledgments

This work was financially supported by the Science & Technology Innovation Talents in Universities of Henan Province (No. 13HASTIT012), the College Outstanding Teachers Program of Henan Province (No. 2012GGJS-128), the Scientific Research Foundation for the Returned Overseas Chinese Scholars of the State Education Ministry, and the Science and Technology Key Project of Henan Education Department (No. 12A150020).

References

[1] L. Sun, C. Tian, M. Li, X. Meng, L. Wang, R. Wang, J. Yin, H. Fu, J. Mater. Chem. A 1 (2013) 6462–6470.
[2] L. Wang, Z. Schnepp, M.M. Titirici, J. Mater. Chem. A 1 (2013) 5269–5273.
[3] M. Biswal, A. Banerjee, M. Deo, S. Ogale, Energy Environ. Sci. 6 (2013) 1249–1259.
[4] X. He, P. Ling, J. Qiu, M. Yu, X. Zhang, C. Yu, M. Zheng, J. Power Sources 240 (2013) 109–113.
[5] H. Jin, X. Wang, Z. Gu, J. Polin, J. Power Sources 236 (2013) 285–292.
[6] X. Liu, M. Zheng, Y. Xiao, Y. Yang, L. Yang, Y. Liu, B. Lei, H. Dong, H. Zhang, H. Fu, ACS Appl. Mater. Interfaces 5 (2013) 4667–4677.
[7] H. Sun, W. He, C. Zong, L. Lu, ACS Appl. Mater. Interfaces 5 (2013) 2261–2268.
[8] X. He, P. Ling, M. Yu, X. Wang, X. Zhang, M. Zheng, Electrochim. Acta 105 (2013) 635–641.
[9] T.E. Rufford, D. Hulicova-Jurcakova, K. Khosla, Z. Zhu, G.Q. Lu, J. Power Sources 195 (2013) 912–918.
[10] Y. Lv, L. Gan, M. Liu, W. Xiong, Z. Xu, D. Zhu, D.S. Wright, J. Power Sources 209 (2012) 152–157.
[11] H.L. Wang, Z.W. Xu, A. Kohandehghan, Z. Li, K. Cui, X.H. Tan, T.J. Stephenson, C.K. King'ondu, C.M.B. Holt, B.C. Olsen, J.K. Tak, D. Harfield, A.O. Anyia, D. Mitlin, ACS Nano 7 (2013) 5131–5141.
[12] L. Wei, M. Sevilla, A.B. Fuertes, R. Mokaya, G. Yushin, Adv. Energy Mater. 1 (2011) 356–361.
[13] H. Zhu, X. Wang, F. Yang, X. Yang, Adv. Mater. 23 (2011) 2745–2748.
[14] M.M. Titirici, R.J. White, C. Falco, M. Sevilla, Energy Environ. Sci. 5 (2012) 6796–6822.
[15] J. Wang, S. Kaskel, J. Mater. Chem. 22 (2012) 23710–23725.
[16] L. Li, R. Ni, Y. Shao, S. Mao, Carbohydr. Polym. 103 (2014) 1–11.
[17] E. Raymundo-Piñero, M. Cadek, F. Béguin, Adv. Funct. Mater. 19 (2009) 1032–1039.
[18] M. Rose, Y. Korenblit, E. Kockrick, L. Borchardt, M. Oschatz, S. Kaskel, G. Yushin, Small 7 (2011) 1108–1117.
[19] D.D. Zhou, Y.J. Du, Y.F. Song, Y.G. Wang, C.X. Wang, Y.Y. Xia, J. Mater. Chem. A 1 (2013) 1192–1200.
[20] S. Thieme, J. Brückner, I. Bauer, M. Oschatz, L. Borchardt, H. Althues, S. Kaskel, J. Mater. Chem. A 1 (2013) 9225–9234.
[21] D.D. Zhou, H.J. Liu, Y.G. Wang, C.X. Wang, Y.Y. Xia, J. Mater. Chem. 22 (2012) 1937–1943.
[22] Y. Liang, Z. Li, R. Fu, D. Wu, J. Mater. Chem. A 1 (2013) 3768–3773.
[23] K. Xia, Q. Gao, J. Jiang, J. Hu, Carbon 46 (2008) 1718–1726.
[24] L.L. Zhang, Y. Gu, X.S. Zhao, J. Mater. Chem. A 1 (2013) 9395–9408.
[25] L. Wei, G. Yushin, Nano Energy 1 (2012) 552–565.
[26] Y. Li, Z.Y. Fu, B.L. Su, Adv. Funct. Mater. 22 (2012) 4634–4667.
[27] Y. Zhai, Y. Dou, D. Zhao, P.F. Fulvio, R.T. Mayes, S. Dai, Adv. Mater. 23 (2011) 4828–4850.
[28] M.A. Lillo-Ródenas, D. Cazorla-Amorós, A. Linares-Solano, Carbon 41 (2003) 267–275.
[29] M.A. Lillo-Ródenas, J. Juan-Juan, D. Cazorla-Amorós, A. Linares-Solano, Carbon 42 (2004) 1371–1375.
[30] A.J. Romero-Anaya, M. Ouzzine, M.A. Lillo-Ródenas, A. Linares-Solano, Carbon 68 (2014) 296–307.
[31] C.R. Pérez, S.H. Yeon, J. Ségalini, V. Presser, P.L. Taberna, P. Simon, Y. Gogotsi, Adv. Funct. Mater. 23 (2013) 1081–1089.
[32] X.Y. Chen, C. Chen, Z.J. Zhang, D.H. Xie, Ind. Eng. Chem. Res. 52 (2013) 12025–12031.
[33] L. Zhao, N. Baccile, S. Gross, Y. Zhang, W. Wei, Y. Sun, M. Antonietti, M.M. Titirici, Carbon 48 (2010) 3778–3787.
[34] A.C. Ferrari, J. Robertson, Phys. Rev. B 61 (2000) 14095–14107.
[35] A.C. Ferrari, J. Robertson, Phys. Rev. B 64 (2001) 075414–075425.
[36] S.K. Meher, P. Justin, G.R. Rao, Nanoscale 3 (2011) 683–692.
[37] S. Park, R.S. Ruoff, Nat. Nanotechnol. 4 (2009) 217–224.
[38] A.V. Neimark, Y. Lin, P.I. Ravikovitch, M. Thommes, Carbon 47 (2009) 1617–1628.
[39] Y.H. Dai, H. Jiang, Y.J. Hu, Y. Fu, C.Z. Li, Ind. Eng. Chem. Res. 53 (2014) 3125–3130.
[40] B. You, J. Yang, Y.Q. Sun, Q.D. Su, Chem. Commun. 47 (2011) 12364–12366.
[41] Z.B. Lei, N. Christov, L.L. Zhang, X.S. Zhao, J. Mater. Chem. 21 (2011) 2274–2281.
[42] Q.G. Shao, J. Tang, Y.X. Lin, F.F. Zhang, J.S. Yuan, H. Zhang, N. Shinya, L.C. Qin, J. Mater. Chem. A 1 (2013) 15423–15428.
[43] J. Wang, L.F. Shen, B. Ding, P. Nie, H.F. Deng, H. Dou, X.G. Zhang, RSC Adv. 4 (2014) 7538–7544.
[44] X.L. Fang, J. Zang, X.L. Wang, M.S. Zheng, N.F. Zheng, J. Mater. Chem. A 2 (2014) 6191–6197.
[45] J.P. Han, G.Y. Xu, B. Ding, J. Pan, H. Dou, D.R. MacFarlane, J. Mater. Chem. A 2 (2014) 5352–5357.